



RESEARCH ARTICLE

10.1029/2024JD042135

Key Points:

- New records and statistical reanalysis reveal an increase in tephra deposition frequency over northeastern North America ca. 9,000 years ago
- This increase likely reflects changing atmospheric circulation associated with the collapse of the Laurentide ice sheet

Supporting Information:

Supporting Information may be found in the online version of this article.

Correspondence to:

A. J. Monteath and B. J. L. Jensen,
alitea@bas.ac.uk;
bjensen@ualberta.ca

Citation:

Monteath, A. J., Jensen, B. J. L., Davies, L. J., Bolton, M. S. M., Hughes, P. D. M., Mackay, H., et al. (2025). Increasing tephra deposition in northeastern North America points to atmospheric circulation changes at the Early Mid Holocene transition. *Journal of Geophysical Research: Atmospheres*, 130, e2024JD042135. <https://doi.org/10.1029/2024JD042135>

Received 4 AUG 2024

Accepted 4 DEC 2024

Author Contributions:

Conceptualization: A. J. Monteath,

B. J. L. Jensen, P. D. M. Hughes

Data curation: A. J. Monteath,

B. J. L. Jensen

Formal analysis: A. J. Monteath,

B. J. L. Jensen, L. J. Davies,

M. S. M. Bolton, H. Mackay, J. Harvey

Funding acquisition: A. J. Monteath,

B. J. L. Jensen, P. D. M. Hughes,

D. G. Froese

Investigation: A. J. Monteath,

B. J. L. Jensen, L. J. Davies, H. Mackay,

J. Harvey, S. Pyne-O'Donnell, C. N. Papp,








G. Mallon, M. J. Amesbury, R. J. Mayfield

Methodology: A. J. Monteath,

B. J. L. Jensen, M. S. M. Bolton

Project administration: A. J. Monteath

Increasing Tephra Deposition in Northeastern North America Points to Atmospheric Circulation Changes at the Early Mid Holocene Transition

A. J. Monteath^{1,2} , B. J. L. Jensen³ , L. J. Davies⁴, M. S. M. Bolton³ , P. D. M. Hughes², H. Mackay⁵, M. E. Edwards², M. Finkenbinder⁶, R. K. Booth⁷ , L. C. Cwynar⁸, J. Harvey³, S. Pyne-O'Donnell⁹, C. N. Papp⁶, D. G. Froese³ , G. Mallon¹⁰ , M. J. Amesbury¹¹, and R. J. Mayfield¹² 

¹British Antarctic Survey, Natural Environment Research Council, Cambridge, UK, ²Geography and Environmental Science, University of Southampton, Southampton, UK, ³Earth and Atmospheric Sciences, University of Alberta, Edmonton, AB, Canada, ⁴Geography, University of Cambridge, Cambridge, UK, ⁵Geography, Durham University, Durham, UK, ⁶Biology and Earth Systems Science, Wilkes University, Wilkes-Barre, PA, USA, ⁷Earth and Environmental Science, Lehigh University, Bethlehem, PA, USA, ⁸Department of Biology, University of New Brunswick, Fredericton, NB, Canada, ⁹Faculty of Social Sciences, Maynooth University, Maynooth, Ireland, ¹⁰Geography, University of Groningen, Groningen, The Netherlands, ¹¹Research Services, University of Exeter, Exeter, UK, ¹²School of Biosciences, University of Nottingham, Nottingham, UK

Abstract The number of cryptotephra (non-visible volcanic ash) records from northeastern North America is unique in the continent. The resulting tephrostratigraphic framework includes ash deposits sourced from volcanic arcs across the Northern Hemisphere and is an exceptional resource for correlating and dating paleoenvironmental records. It also provides an opportunity to explore more novel questions regarding the controls on ultra-distal tephra (volcanic ash >3,000 km from source) dispersal and deposition. Here, we examine temporal patterns in the tephrostratigraphy of northeastern North America to test the legitimacy of a previously noted change in ash deposition frequency at the Early Mid Holocene transition. We integrate five new cryptotephra records into the existing framework to improve its temporal and spatial extent and report further occurrences of widespread cryptotephra deposits including Mt. St. Helens We, Jala pumice, White River Ash east, Ruppert tephra, Mt. St. Helens Yn and Mazama Ash. Reexamination of the combined tephrostratigraphy using breakpoint analysis shows a significant increase in the frequency of ashfall after ca. 9,000 (7,860–9,650) cal yr BP (calendar years before C.E. 1950). We discuss this change in relation to volcanic and environmental controls of fine ash dispersal and preservation. We reject hypotheses relating to eruption frequency or depositional processes in favor of changing atmospheric transport patterns and tephra dispersal—possibly caused by the retreat of the Laurentide Ice Sheet. Our study is a novel example of how tephrostratigraphy can be used beyond traditional correlative and dating studies, in this case indicating large-scale changes in atmospheric circulation through time.

Plain Language Summary Microscopic volcanic ash beds can be traced across continents and in northeastern North America have been extensively studied to form a stratigraphic framework of ashfall spanning the last 16,000 years. In this study, we extend the spatial and temporal extent of this framework and use statistical breakpoint analysis to look for patterns in ashfall frequency through time. We find that there is a sustained increase in the frequency of ashfall around 9,000 years ago. This pattern is inconsistent with wider records of volcanism and depositional processes and can only be explained by changes in atmospheric circulation. Paleoenvironmental records also show evidence for atmospheric changes that were driven by the collapse of the North American ice sheets. Our findings show that distal records of ashfall are sensitive to long-term atmospheric change and can provide new data for testing paleoclimate simulations.

1. Introduction

The characterization and correlation of volcanic ash beds has become a valuable chronological tool in Quaternary science (Lowe, 2011), and detailed tephrostratigraphic frameworks have been developed from diverse regions around the world (e.g., Davies et al., 2016; Fontijn et al., 2014; Lowe et al., 2008; Ponomareva et al., 2017). These frameworks combine multiple study sites to provide a regional tephrostratigraphy (the sequence of tephra

Resources: A. J. Monteath, B. J. L. Jensen, M. Finkenbinder, R. K. Booth, L. C. Cwynar

Supervision: P. D. M. Hughes, M. E. Edwards, D. G. Froese

Visualization: A. J. Monteath

Writing – original draft: A. J. Monteath

Writing – review & editing:

A. J. Monteath, B. J. L. Jensen, M. S. M. Bolton, P. D. M. Hughes, H. Mackay, M. E. Edwards, M. Finkenbinder, L. C. Cwynar

deposits; Lowe & Hunt, 2001; Thorarinsson, 1981), which can be used to refine chronologies and provide tie-points between paleoenvironmental or archeological sequences. In addition to their applications in Quaternary research, tephrostratigraphic frameworks are fundamental for developing estimates of eruption frequency and magnitude, as well as informing ash-dispersal hazard assessments and climate models (e.g., Cashman & Rust, 2020; Mackay et al., 2022; Saxby et al., 2020; Watson, Swindles, Savov, et al., 2017). More recently, improved protocols for the extraction and analysis of volcanic glass have allowed cryptotephra deposits (non-visible volcanic ash) to be routinely identified and correlated between sedimentary sequences (e.g., Blockley et al., 2005; Dugmore et al., 1995; Eden et al., 1992; Hayward, 2012; Pilcher & Hall, 1992; Turney, 1998). This has expanded tephrostratigraphic frameworks both spatially and temporally, and volcanic ash can now be traced across continents (e.g., Jensen et al., 2014; Pearce et al., 2004; Plunkett & Pilcher, 2018). As a result of these advances, regional cryptotephra frameworks have been established independently of proximal deposits—in some cases thousands of kilometers from the source volcanoes and including tephra deposits that are not present in proximal areas (e.g., Jensen et al., 2021; Timms et al., 2019). These distal tephra frameworks provide a record of ash dispersal that exceeds historical observations (Swindles et al., 2011), and recent studies have investigated spatial and temporal patterns in the distribution of cryptotephra deposits to better understand (and predict) volcanic hazards (e.g., ash cloud return intervals; Lawson et al., 2012; Sulpizio et al., 2014; Swindles et al., 2011, 2018; Watson, Swindles, Savov, et al., 2017). To date, such studies have been limited to Europe, a region with a long history of cryptotephra research and a high density of study sites (e.g., Dugmore, 1989; Persson, 1971; Pilcher et al., 1995; Plunkett et al., 2004); however, there is clearly potential to use this approach in other regions that are affected by tephra deposition. Because tephra deposits tend to be geochemically distinct and can be traced back to source, they also provide an opportunity to examine atmospheric circulation patterns that is complementary to dust records and other proxies. Surprisingly, few studies have explored this avenue of research with most examples limited to Greenland and Antarctica (e.g., Lacasse, 2001; Narcisi et al., 2005, 2012). However, the last decade has seen an explosion in tephra research that has rapidly increased the density and geographic extent of tephra records, which lays the groundwork for exploring these more novel applications.

1.1. Ultra-Distal Cryptotephra Deposition in Northeastern North America

The number of cryptotephra records from northeastern North America is higher than anywhere in the continent despite the comparatively short period of study. Pyne-O'Donnell et al. (2012) reported the first cryptotephra record from this region and identified numerous ultra-distal ash deposits (volcanic ash >3,000 km from source) in Nordan's Pond Bog, Newfoundland (Figure 1). These cryptotephra deposits were correlated with volcanic eruptions in Alaska and the Cascade Range that took place up to 7,000 km from Newfoundland and began a new interest in tephra dispersal in North America. Since the publication of this first record, a series of studies have closely examined the lake, peat and ocean sediments of northeastern North America for the presence of volcanic ash (Jensen et al., 2014, 2021; Mackay et al., 2016, 2022; Monteath, Teuten, et al., 2019; Monteath et al., 2023; Pyne-O'Donnell et al., 2016; Rabett et al., 2019; Spano et al., 2017). These studies have identified numerous cryptotephra deposits sourced from volcanoes around the Pacific north-west and Mexico, some of which have also been found in the Greenland ice cores (Coulter et al., 2012; Pearce et al., 2004; Zdanowicz et al., 1999) and western Europe (Jensen et al., 2014, 2021; Jones et al., 2020; Kinder et al., 2020; Plunkett & Pilcher, 2018; Pyne-O'Donnell & Jensen, 2020; Watson, Kołaczek, et al., 2017; Watson, Swindles, Lawson, et al., 2017). Several of these deposits were formed during vast caldera-forming events (e.g., Mazama Ash, ~176 km³ erupted volume, Buckland et al., 2020) while others were produced by comparatively small eruptions (e.g., South Mono, ~0.2 km³ erupted volume, Bursik et al., 2014)—suggesting that factors other than magnitude, such as duration and atmospheric circulation patterns, play important roles in the dispersal of distal tephra. This work recently advanced considerably with the development of a new integrated tephrostratigraphic framework for the region that compiled previous studies with new sites, geochemical analyses, and updated age models (Jensen et al., 2021). The comprehensive network of sites, distributed from the USA Midwest to coastal Newfoundland and Maine, contains cryptotephra deposits sourced from nearly every major volcanic arc in eastern Eurasia and North America and provides an opportunity to explore questions beyond 'traditional' tephrochronology. This includes, but is not limited to, examining what tephra deposits may be able to tell us about controls on ash distribution and preservation.

One of the most striking patterns recorded in the tephrostratigraphic framework of northeastern North America is an apparent sustained increase in the frequency of cryptotephra deposition around the Early to Middle Holocene boundary (8,200 cal BP; Greelandian-Northgrippian; Walker et al., 2019), beginning with Mazama Ash, ca.

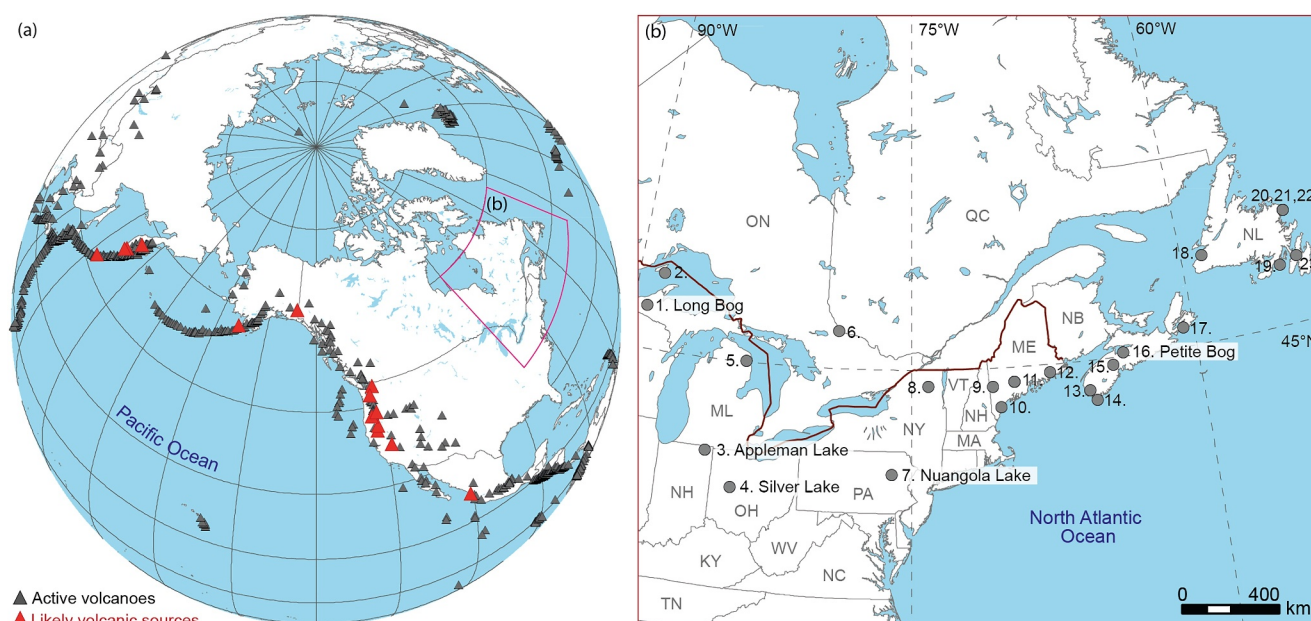


Figure 1. (a) Volcanic regions affecting northeastern North America. Black triangles represent active (Quaternary) volcanoes. Red triangles represent volcanoes linked with cryptotephra deposits in northeastern North America. (b) The location of new sites (labeled) from this study and published cryptotephra records in northeastern North America that are numbered west to east: (1) Long Bog, (2) Lake Superior, (3) Appleman Lake, (4) Silver Lake, (5) Irwin Smith Bog, (6) Balsam Creek, (7) Nuangola Lake, (8) Bloomingdale Bog, (9) Crocker Pond, (10) Saco Heath, (11) Sidney Bog, (12) Great Heath Bog, (13) Thin-ice Pond, (14) Villagedale Bog, (15) Veinot Lake, (16) Petite Bog, (17) Framboise Bog, (18) Jeffrey's Bog, (19) Placentia Bay, (20) Nordan's Pond Bog, (21) Southwest Pond Bog, (22) Pound Cove Bog and (23) Baby Pond Bog. Site numbering corresponds with Table 1.

$7,572 \pm 18$ cal yr BP (Sigl et al., 2022). This pattern was first noted in Nordan's Pond Bog, Newfoundland, by Pyne-O'Donnell et al. (2012) who hypothesized that the increase in cryptotephra deposition “may reflect reorganizations of atmospheric circulation patterns and airflow strength across the continent perhaps under the diminishing influence of the decaying Laurentide Ice Sheet.” Subsequently, Jensen et al. (2021) noted similar results in cores from Sidney Bog and Thin Ice Pond (Figure 1); however, the number of regional cryptotephra records spanning the late Pleistocene and Early Holocene is limited, making any conclusions about the replicability and cause of this apparent pattern premature. Here, we test the hypothesis of Pyne-O'Donnell et al. (2012) in a novel example of how distal tephra deposition can be used to examine past climatic processes.

2. Materials and Methods

In this study, we add five new cryptotephra records to the regional tephrostratigraphy of northeastern North America to improve the temporal and spatial extent of this framework (Figure 1; Table 1; Supplementary Text S1.1 in Supporting Information S1). We then examine changes in the frequency of cryptotephra deposition between ca. 16,000 cal yr BP and today. Finally, we raise hypotheses regarding fine ash production, dispersal, and preservation in northeastern North America that may explain the pattern first observed by Pyne-O'Donnell et al. (2012).

2.1. Compiling and Integrating Cryptotephra Records

We quantified shard abundance in our new study sites using standard protocols (e.g., Pilcher & Hall, 1992; Turney, 1998) and analyzed the major-minor element composition of cryptotephra deposits using electron probe microanalysis (EPMA) with wavelength dispersive spectrometry. For each study site, we developed a Bayesian age-depth model using OxCal v.4.4.4 (Bronk Ramsey, 2009a, 2009b) and the IntCal20 Northern Hemisphere radiocarbon calibration curve (Reimer et al., 2020). We also developed new age-depth models for study sites described by Gill et al. (2009, 2012); Pyne-O'Donnell et al. (2016), Mackay et al. (2016) and Rabett et al. (2019), using the same methods, in order to use the most recent radiocarbon calibration curve (IntCal20; Reimer et al., 2020; Figures S1, S2 in Supporting Information S1). Detailed descriptions of methods and new

Table 1

New and Published Northeastern North America Cryptotephra Records Discussed in the Text

| n. | Study site | Lat | Long | Time span ^a (cal yr BP) | Setting | Reference(s) |
|----|----------------------------|-------|--------|------------------------------------|----------|---|
| 1 | Long Bog | 46.00 | −89.72 | 12,000–16,500 | Peat-bog | This study |
| 2 | Lake Superior ^b | 47.13 | −87.82 | Undated | Lake | Spano et al. (2017) |
| 3 | Appleman Lake | 41.62 | −85.21 | 14,800–17,700 | Lake | Gill et al. (2009), This study |
| 4 | Silver Lake | 40.35 | −83.81 | 16,000–10,200 | Lake | Gill et al. (2012), This study |
| 5 | Irwin Smith Bog | 45.03 | −83.62 | 6,600-modern | Peat-bog | Jensen et al. (2021) |
| 6 | Balsam Creek | 46.48 | −79.15 | 10,500-modern | Lake | Rabett et al. (2019) |
| 7 | Nuangola Lake | 41.16 | −75.97 | 15,300-modern | Lake | This study |
| 8 | Bloomington Bog | 44.38 | −74.14 | 7,700-modern | Peat-bog | Jensen et al. (2021) |
| 9 | Crocker Pond | 44.31 | −70.82 | 13,900–12,800 | Lake | Pyne-O'Donnell et al. (2016) |
| 10 | Saco Heath | 43.55 | −70.03 | 7,000-modern | Peat-bog | Mackay et al. (2016) |
| 11 | Sidney Bog | 44.39 | −69.79 | 10,900-modern | Peat-bog | Jensen et al. (2021) |
| 13 | Thin-ice Pond | 43.91 | −65.86 | 14,500–4,200 | Lake | Pyne-O'Donnell et al. (2016); Jensen et al. (2021) |
| 14 | Villagedale Bog | 43.52 | −65.53 | 6,000-modern | Peat-bog | Mackay et al. (2016); This study |
| 15 | Veinot Lake | 44.74 | −64.54 | 14,500–11,300 | Lake | Pyne-O'Donnell et al. (2016) |
| 16 | Petite Bog | 45.14 | −63.94 | 13,500-modern | Peat-bog | Jensen et al. (2014); Charman et al. (2015); This study |
| 17 | Framboise Bog | 45.72 | −60.55 | 10,200-modern | Peat-bog | Mackay et al. (2016) |
| 18 | Jeffrey's Bog | 48.21 | −58.82 | 3,500-modern | Peat-bog | Mackay et al. (2016) |
| 19 | Placentia Bay | 47.23 | −54.61 | 10,000-modern | Ocean | Monteath et al. (2023) |
| 20 | Nordan's Pond Bog | 49.16 | −53.60 | 9,600-modern | Peat-bog | Pyne-O'Donnell et al. (2012); Jensen et al. (2021) |
| 21 | Southwest Pond Bog | 49.12 | −53.72 | 4,300-modern | Peat-bog | Mackay et al. (2022) |
| 21 | Pound Cove Bog | 49.27 | −53.59 | 8,000 | Peat-bog | Blundell et al. (2018); Monteath, Teuten, et al. (2019); Mackay et al. (2022) |
| 23 | Baby Pond Bog | 47.42 | −53.55 | Undated | Peat-bog | Monteath, Teuten, et al. (2019) |

^aTime span refers to period covered by cryptotephra counts. ^bSpano et al. (2017) report two nearby cryptotephra records from Superior Lake. Numbering (n.) corresponds with Figure 1.

data, including secondary standard measurements, are available in Supplementary Information (Supplementary Text S1 and Supplementary Tables S1–S5 in Supporting Information S1).

2.2. Quantifying Primary Ashfall Events

Ideally, a cryptotephra deposit identified in sediment represents a primary ashfall event, but various environmental and post-depositional processes can have large impacts on the distribution of these microscopic deposits (e.g., Davies et al., 2005; Mackay et al., 2016; Monteath, Hughes, & Wastegård, 2019; Pyne-O'Donnell., 2011). Therefore, defining primary ashfall events can become subjective if EPMA data are limited or include multiple populations that could represent either reworking, several primary airfall events shortly spaced in time, or both. Volcanic glass is ubiquitous in many deposits and therefore multiple, consistent EPMA data are needed to infer the presence of a primary airfall. Where low numbers of EPMA data points are available, it is important to consider a range of factors, including, but not limited to the following: the depositional environment (e.g., lake, ombrotrophic peat-bog, fen), sediment accumulation rate, mechanisms for reworking (e.g., inflow from surrounding basin, bioturbation by microfauna or post-depositional root penetration), presence of wind-blown sediment (e.g., loess), repetition of geochemical populations at varying depths, amount of weathered and/or detrital grains, the uniqueness of a geochemical population, and supporting information such as radiocarbon dates and potential correlations with previously reported tephra deposits (Jensen et al., 2021; Lowe et al., 2017). All of these processes complicate data and introduce uncertainty when quantifying the number of primary ashfall events.

To mitigate this, we quantified the number of ashfall events using two different methods. The first only includes cryptotephra deposits that can confidently be described as primary based on clearly defined shard peaks, sufficient

coherent EPMA data (≥ 4 analyses) and a consistent depositional environment (i.e., no sudden changes in accumulation rate or sedimentation regime). The second includes all cryptotephra deposits that could plausibly be defined as primary ashfall events, including diffuse, or low shard counts, and multiple glass major-minor element populations with limited EPMA data (Figure S9 in Supporting Information S1). In effect, these contrasting approaches produce the ‘minimum’ and ‘maximum’ number of primary ashfall events in our records. We excluded records that only targeted depth intervals around single cryptotephra deposits (e.g., Lake Superior, Pound Cove Bog, Southwest Pond Bog and Baby Pond Bog; Mackay et al., 2022; Monteath, Teuten, et al., 2019; Spano et al., 2017) and results from the ocean-sediment core AI07-10G, Placentia Bay, Newfoundland (Monteath et al., 2023), as ocean cores are subject to different depositional processes than terrestrial cores as well as radiocarbon reservoir effects.

Cryptotephra deposits from disparate sites were combined as unified site-averaged cumulative airfall curves. In short, the median ages for confidently identified primary ashfall events (i.e., ‘minimum ashfall number’) were assigned to individual 500-year bins, approximating the average 95% high-density ranges of modeled cryptotephra deposits. The counts per bin were then normalized based on the number of sites encompassing that interval. This process was then repeated, including all plausible tephra events (i.e., ‘maximum ashfall number’). Finally, breakpoint analysis was conducted following the segmented regression protocol of Muggeo (2003, 2008) with the number of breakpoints selected by optimizing the Bayesian Information Criterion (Muggeo, 2020). The timing of breaks in the segmented relationships for ‘minimum’ and ‘maximum’ cryptotephra occurrences revealed when substantial regime shifts in the deposition trends occurred, whereas the slope of the segments was the average tephra deposition rate (i.e., deposits per year). In addition to the regime-shift models, which approximate cumulative airfall frequency, we tested alternative hypotheses regarding cryptotephra deposit detection per bin. We developed two simple intercept-free linear models.

1. **Total Sites Model:** Predicts ‘minimum’ or ‘maximum’ cryptotephra deposit counts in each bin based on a scaling relationship with the total number of sites (all types) sampling an interval.
2. **Site Type Model:** Predicts ‘minimum’ or ‘maximum’ cryptotephra deposit counts per bin using a two-term additive scaling relationship based on the number of bog-type or lake-type sites sampling an interval.

In both models, the scaling parameters for total sites or peat-bog and lake sites are constrained to be non-negative. These models, were also corrected for sampling intensity and their uncertainty was propagated during conversion to cumulative airfall curves for comparison with the regime-shift model(s).

3. Results

3.1. New Cryptotephra Records

Our data includes new occurrences of well-characterized wide-spread cryptotephra deposits that have previously been identified in northeastern North America. These include Mt. St. Helens We, Jala pumice, White River Ash east, Ruppert tephra, Mt. St. Helens Yn and Mazama ash (Supplementary Text S2.1 and Figures S4–S6 in Supporting Information S1). More tentative links are made with SB-13/T317 in Sidney Bog and Thin Ice Pond (Figure S7 in Supporting Information S1; Jensen et al., 2021) as well as a Mid Holocene eruption of Shiveluch (Figure S7 in Supporting Information S1). Several uncorrelated EPMA populations may represent new regional occurrences of cryptotephra deposits, however, cannot be linked with volcanic sources based on available data (Table S1 in Supporting Information S1). This includes Cryptotephra deposits SL_882a from Silver Lake, which may have an Icelandic provenance (Figure S8 in Supporting Information S1).

3.2. Temporal Patterns in Cryptotephra Deposits

Across the 18 available sites, we find strong evidence for 45 ashfall events in northeastern North America during the last 16,000 years based on shard counts, chronology, and glass EPMA data (Supplementary Information, Tables S4 and S5 in Supporting Information S1). Forty of these events occurred between ca. 8,000 cal yr BP to present, whereas only five predate this: SL_882a (15,100–13,800 cal yr BP; this study), Glacier Peak B, Glacier Peak G (13,710–13,410 cal yr BP; Pyne-O'Donnell et al., 2016), Mt. St. Helens J (13,800–12,800 cal yr BP; Pyne-O'Donnell et al., 2016), and an uncorrelated cryptotephra deposit from Balsam Creek (9,370–8,100 cal yr BP; Rabett et al., 2019). The frequency of cryptotephra deposition events undergoes a step change around 9,000 cal yr BP (Figure 2) from one airfall event per 1,600 years between 16,000–18,000 cal yr BP to one airfall event per

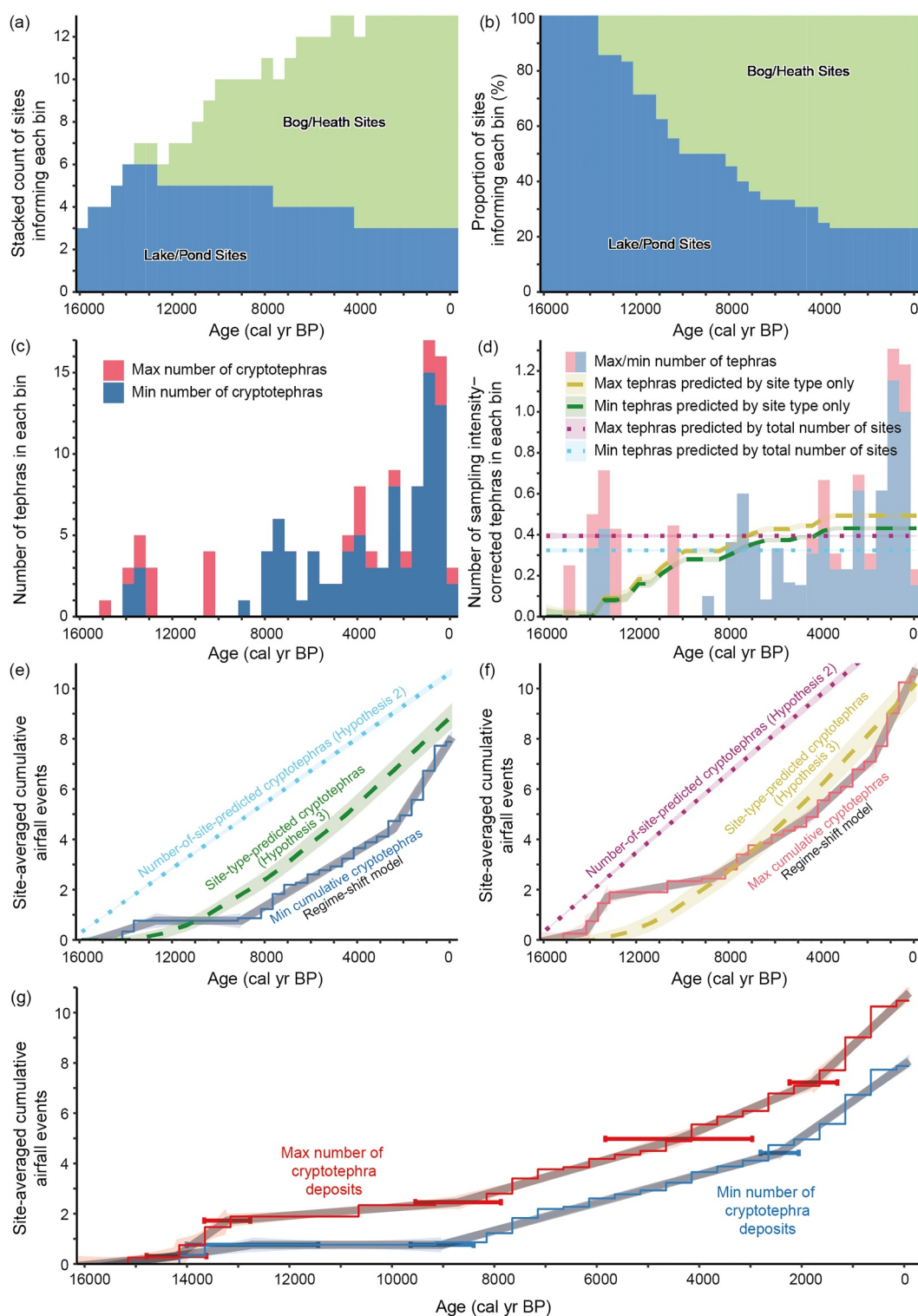


Figure 2. (a), (b) Composite plots depicting site coverage and site type. (c), (d) Minimum and maximum airfall events as a histogram with two explanatory models for cryptotephra deposition at peat and lacustrine core sites in eastern North America. (e), (f) Minimum and maximum airfall events as a cumulative counts with two explanatory models for cryptotephra deposition at peat and lacustrine core sites in eastern North America. (g) Minimum and maximum site-averaged cumulative airfall events shown with 95% confidence intervals for change-point locations in the segmented regression (i.e., “regime-shift model”). All shaded envelopes indicate 95% confidence intervals.

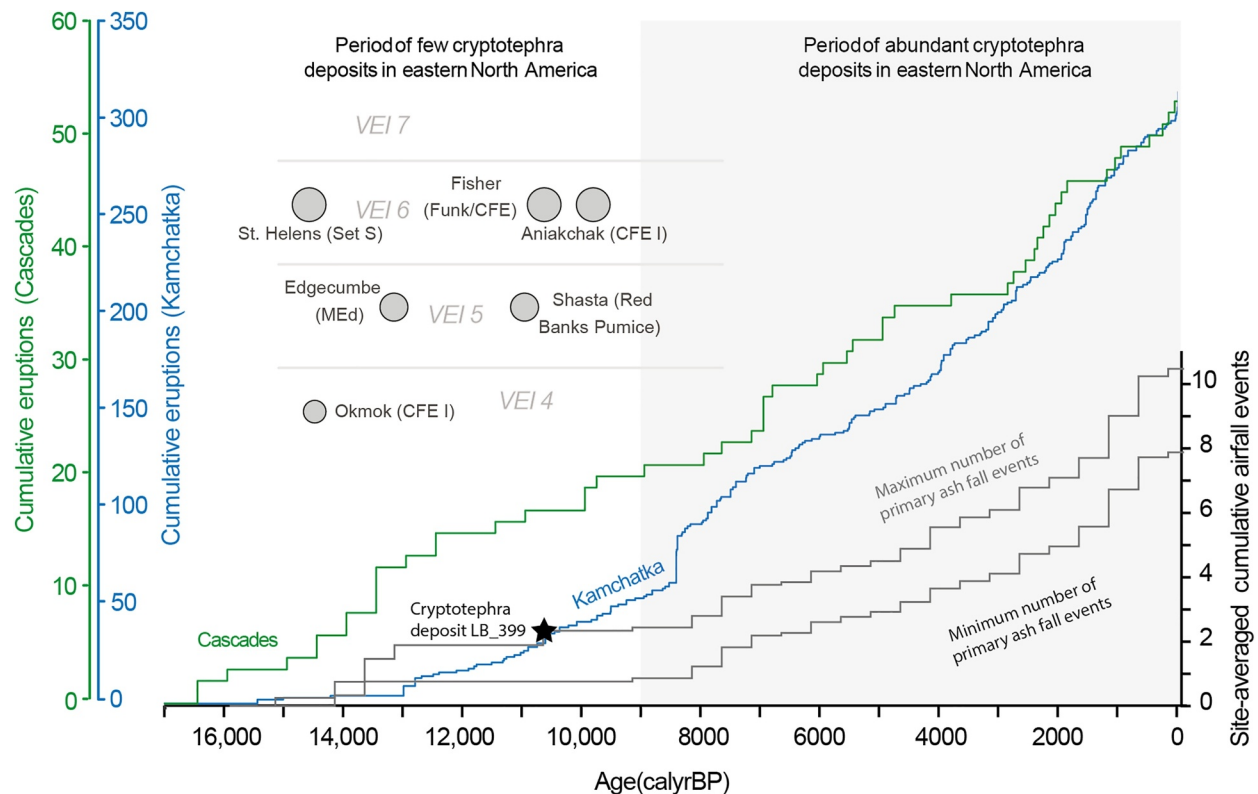


Figure 3. Cumulative numbers of eruptions from Kamchatka (shown in blue) and the Cascades (shown in green) plotted against the site-average cumulative number of cryptotephra deposits in northeastern North America (Portnyagin et al., 2020; Watt et al., 2013). Notable eruptions that are not present in the northeastern North America tephrostratigraphy are shown as filled circles at their approximate age with circle size and vertical position corresponding to their estimated Volcanic Explosivity Index (VEI; Newhall & Self, 1982).

200 years between 8,000 cal yr BP to present (based on number of unique tephra deposits). During the last 1,000 years, there is strong evidence for 10 ashfall events—a return interval of approximately 100 years. This compares with an ashfall return interval of 44 ± 7 years in north-western Europe during the same period (Watson, Swindles, Savov, et al., 2017).

We find weaker evidence for a further 19 ashfall events in northeastern North America based on minor glass EPMA populations (Tables S4 and S5 in Supporting Information S1). These populations are often mixed with EPMA data from primary ashfall events, reworked glass, or detrital/weathered glass and so cannot be confidently described as primary ashfall events. Including these minor glass EPMA populations in our quantification of ashfall frequency has very little effect on the pattern observed in the cumulative number of cryptotephra deposits. Although both the ‘minimum’ and ‘maximum’ site-averaged cumulative airfall curves display multiple (three to five) breakpoints as selected by Bayesian information criterion (Figure 2), each cumulative airfall curve exhibits tephra accumulation acceleration around the weighted mean 8,864 cal yr BP (± 265 years $1-\sigma$) with upper and lower ranges between 7,855 and 9,648 cal yr BP at the $2-\sigma$ level. The mean timing difference between the ca. 9,000 cal yr BP breakpoints in the ‘minimum’ tephra and ‘maximum’ tephra scenarios is only 314 years (± 529 years $1-\sigma$). Although the overall picture of tephra accumulation rates is similar under the ‘minimum’ and ‘maximum’ tephra assumptions, the rate of accumulation is inherently higher for the maximum tephra curves. For example, at 6,000 cal yr BP the cryptotephra deposit rates every millennium are 0.56 ± 0.03 years $^{-1}$ for the ‘minimum’ cumulative airfall curve and 0.59 ± 0.06 years $^{-1}$ for the ‘maximum’ cumulative airfall curve. (See Figure 3).

The most substantial difference between the ‘minimum’ tephra and ‘maximum’ estimates of ashfall frequency is caused by the cryptotephra deposit LB_399, in Long Bog (Figure 2). Inclusion of this cryptotephra deposit results in a steeper site-averaged cumulative airfall curve prior to ca. 9,000 cal yr BP and a later breakpoint as selected by

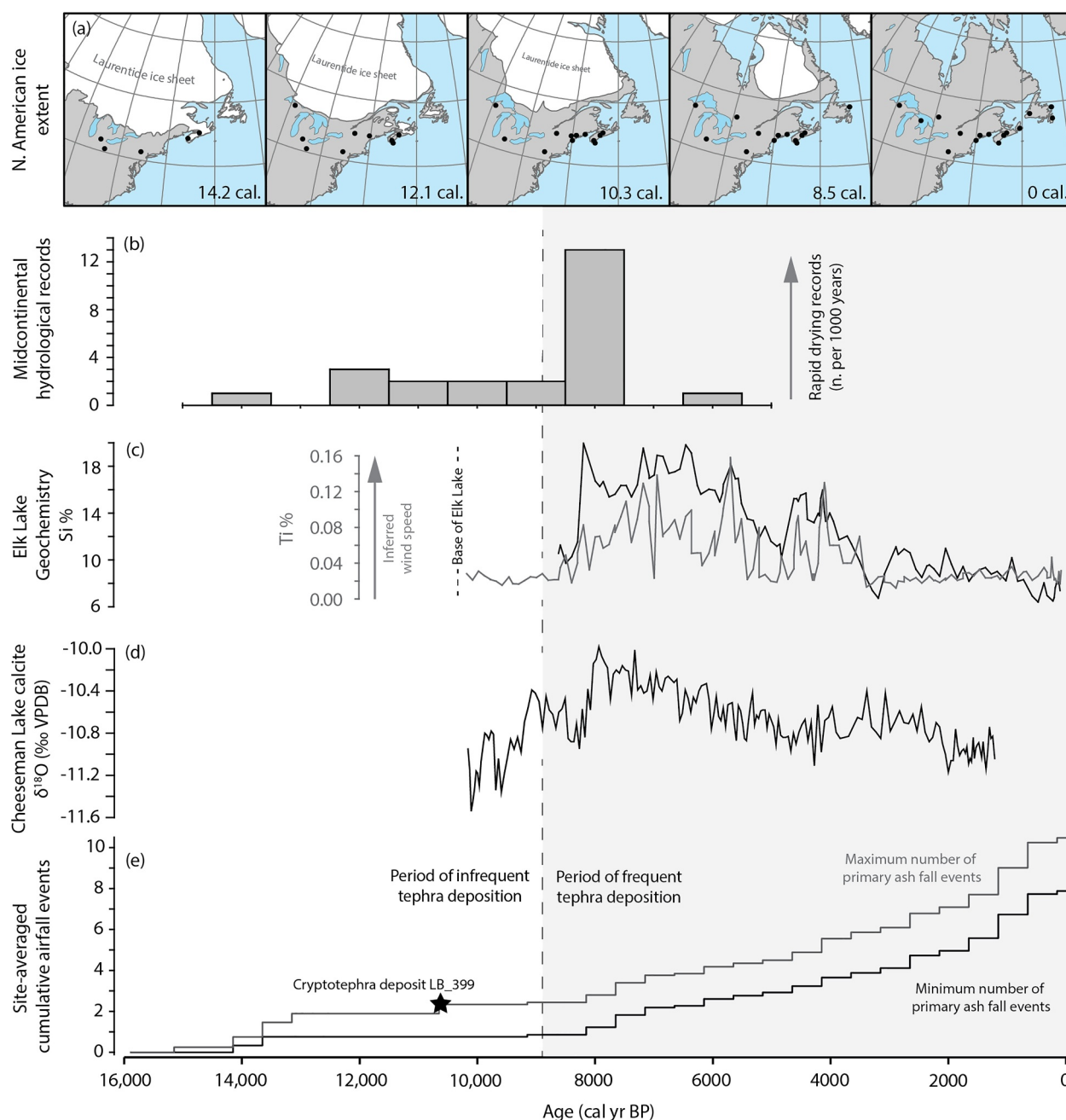


Figure 4. (a) North American ice extent (Dalton et al., 2020). Cryptotephra records are indicated as gray circles. (b) USA midcontinental hydrological records (inferred from pollen, isotopic, aeolian and paleohydrological proxies; Williams et al., 2010). (c) Elk Lake, Minnesota, geochemistry—where increasing Ti and Si represent elevated dust levels and strengthening wind speed (Dean et al., 2002). (d) Cheeseman Lake, Newfoundland, calcite $\delta^{18}\text{O}$ values. (Finkenbinder et al., 2016) (e) Site-averaged cumulative airfall events in northeastern North America.

Bayesian information criterion (Figure 2). LB_399 is dated to ca. 10,400 cal yr BP and is predominately formed of re-worked or weathered glass shards (30 of the 44 EPMA analyses). Within the EPMA data, however, are four minor populations ($n = 5$, $n = 3$, $n = 3$ and $n = 3$). Although these analyses show similarities with EPMA data from Holocene eruptions, there are substantial differences in ages of these eruptions and LB_399 (Supplementary Information, Table S1 in Supporting Information S1). Given the dominance of reworked glass, limited consistent EPMA data and absence of any plausible correlation, we consider it very unlikely that LB_399 represents primary airfall tephra; however, we include it in our ‘maximum estimate’ of cryptotephra deposits for completeness. (See Figure 4).

Although much of our results draw from the segmented regression “regime-shift” model, with rates of change derived from that analysis due to its close match with the observed cumulative airfall curves (Figures 2e–2g), we also study the predicted cumulative airfall curves from our two intercept-free site-coverage scaling models (Figures 2d–2f). As a result of its formulation, the intensity-corrected number of cryptotephra deposits modeled by the “total sites” model is uniform (Figure 2b). Therefore, the cumulative curves from these models are linear and, as a result, cannot replicate the irregular tephra deposition rates observed in our records and modeled by our regime shift models (Figures 2e and 2f). The “site-type” model is more flexible, but still shows substantial dissimilarity with our observed cryptotephra cumulative curves (e.g., ca. 3,000 cal yr BP for the ‘minimum’ cryptotephra curve; ca. 12,000 cal yr BP for the ‘maximum’ cryptotephra curve; Figures 2e and 2f, respectively). One curious result is that in both the minimum- and maximum-tephra site-type models, the coefficient for lake sites is 0 on average (i.e., the lake term is eliminated from predictions before intensity correction; lake coefficient standard errors for minimum and maximum models are 0.2027 and 0.1713, respectively). Although the zero coefficient is “optimal” in that it best predicts cryptotephra counts, the site-type model is likely to be misspecified since we observe cryptotephra deposits in lake sites even when no peat-bog cores inform a given bin.

4. Discussion: What Caused the Increase in Tephra Deposition Frequency Around 9,000 cal yr BP?

Our results show that the initial observation of a distinct step change in the frequency of tephra deposition at Nordan's Pond ca. 8,000 cal yr BP (Pyne-O'Donnell et al., 2012) is replicated across northeastern North America with an inflection point around 9,000 cal yr BP in our regional compilation. There are several plausible explanations for this observation and the following sections explore four hypotheses.

4.1. Hypothesis 1: The Increase in the Frequency of Cryptotephra Deposits Was Caused by an Increase in Eruption Frequency

The increase in the frequency of cryptotephra deposits after ca. 9,000 cal yr BP could be explained by an increase in the number of explosive eruptions, that is, if more large explosive eruptions took place in the volcanic source regions, we would expect to see more ultra-distal cryptotephra deposits preserved in northeastern North America. However, the available geologic evidence is discordant with this hypothesis. Studies of proximal tephra deposits from the regions affecting northeastern North America demonstrate that numerous large eruptions took place throughout the time period spanned by our records (Hildreth, 2007; Kyle et al., 2011; Miller & Smith, 1987; Mullineaux, 1996; Portnyagin et al., 2020, Figure 3; Watt et al., 2013). Databases of large volcanic eruptions (LaMEVE; Crosweller et al., 2012; Global Volcanism Program, 2018) do show a global upturn in volcanism following the onset of the Holocene and again during the Late Holocene. However, these increases are likely to reflect a geographical bias in the recording of evidence for past eruptions (e.g., toward regions with long historical records) rather than physical processes (Brown et al., 2014). Conversely, the SO₄ records from the Greenland ice cores suggest that volcanism increased during the late Pleistocene and Early Holocene (Sigl et al., 2022; Zielinski et al., 1996, 1997), which is not reflected in the tephrostratigraphy of northeastern North America. This increase is suggested to have been driven by crustal unloading as Pleistocene ice-sheets retreated (Jull & McKenzie, 1996), and although the Greenland ice core record is biased toward Icelandic eruptions there is also evidence for intensified volcanism in several of the high-latitude volcanic regions affecting northeastern North America during this period (Alaska and Kamchatka; Braitseva et al., 1995; Brown et al., 2014; de Fontaine et al., 2007; Praetorius et al., 2016). Therefore, the available evidence does not support Hypothesis 1, and the temporal pattern of tephra deposition evident in northeastern North America is unlikely to represent an increase in volcanic activity after ca. 9,000 years BP.

4.2. Hypothesis 2: The Increase in the Frequency of Cryptotephra Deposits Was Caused by Bias in the Number of Available Study Sites or EPMA Data

The increase in the frequency of cryptotephra deposits after ca. 9,000 cal yr BP may reflect a bias in the number of available study sites or number of glass major-minor element analyses. The cryptotephra framework in northeastern North America was not developed to investigate temporal patterns in ashfall events. Although we have analyzed new study sites for this purpose (principally through the investigation of late Pleistocene and Early Holocene records), a bias toward Mid to Late Holocene records remains (Figure S3 in Supporting

Information S1). It is possible that the higher frequency of cryptotephra deposits between ca. 9,000 cal yr BP to present day reflects the increased study-site density for this period. We consider this unlikely, however, for two reasons. First, the Bayesian information criterion break point in the cumulative site-averaged ashfall events ca. 9,000 cal yr BP does not coincide with a sudden increase in the number of study sites (Figure S3 in Supporting Information S1). Second, the late Pleistocene and Early Holocene cryptotephra records are numerically distinct from younger periods. For example, site coverage during the time-period between 14,000 cal yr BP and 8,000 cal yr BP (6,000 years) is never less than five records and includes only four confidently identified ashfall events. During the Mid to Late Holocene, no combination of five records covering 6,000 years includes less than eight confidently identified ashfall events.

By correcting cryptotephra counts per bin by the number of sites available, we implicitly account for sampling coverage. However, we also explicitly evaluated the degree to which the number of sample sites could predict cryptotephra frequency. Without fundamentally changing the formulation of our “total sites” model, a consistent deposition rate must always be found once we correct for sampling intensity, and this appears at odds with the fluctuating rates of deposition found in northeastern North America (Figure 2). Our detecting *any* significant breaks in slope in the intensity-corrected segmented regression is evidence against the notion that the number of cryptotephra deposits in each bin over time is effectively predicted by the number of sites representing each bin. An alternative approach to testing this model would attempt to regenerate the change rate from the mean minimum and maximum intensity-corrected tephra counts per bin. However, this also gives no slope breaks, necessitating a mismatch from our records.

We recognize the availability of EPMA data is biased toward the Mid to Late Holocene as this period has been studied in greater detail. In this study, we have gone some way to address this by making a concerted effort to identify the late Pleistocene Glacier Peak and Mt. St. Helens J eruptions. Despite diffuse/low shard counts and, in Long Bog, abundant background tephra, we undertook 211 EPMA analyses on poorly defined Pleistocene shard peaks as low as 4 shards per gram to try and locate these marker horizons (Supplementary Tables S1 and S4 in Supporting Information S1). It is likely that further Mid to Late Holocene cryptotephra deposits would be identified if similar comprehensive EPMA strategies were followed in all records—further emphasizing the pattern of increasing tephra deposition after ca. 9,000 cal yr BP.

4.3. Hypothesis 3: The Increase in the Frequency of Cryptotephra Deposits Was Caused by Depositional Environments/Processes

We consider the possibility that the increase in the frequency of cryptotephra deposits after ca. 9,000 cal yr BP was caused by differing depositional environments and/or depositional processes. The Middle to Late Holocene tephrostratigraphy of northeastern North America is mainly derived from peat-bogs. In contrast, the late Pleistocene and Early Holocene tephrostratigraphy is mostly developed from lakes as these began to accumulate sediment earlier than regional peat initiation following deglaciation (Jensen et al., 2021; Pyne-O'Donnell et al., 2016; this study). The change in analyzed depositional environment could cause an apparent increase in the frequency of cryptotephra deposits if one deposit type was more effective at preserving cryptotephra deposits. This hypothesis is not supported by the published literature, however, as both peat-bogs and lakes have repeatedly been shown to be good archives of distal cryptotephra deposits that preserve common isochrons (e.g., Jensen et al., 2021; Timms et al., 2019; Watson et al., 2016). This includes Nuangola Lake from this study, which spans ca. 16,000–0 cal yr BP and preserves multiple discrete cryptotephra deposits, including an abundant WRAe ash deposit composed of >16,000 shards per gram (Table S4 in Supporting Information S1). The Nuangola Lake record also shows the same pattern as the wider data set with no cryptotephra tephra deposits prior to the Early Mid Holocene transition and multiple deposits after.

Our site-type-based model fails to replicate the slope changes in the cumulative airfall curves of Figure 2. It should also not be misconstrued that, owing to zero coefficient, lakes negligibly contribute to the cryptotephra record. Our study does not directly test the cryptotephra productivity of concomitant lake and peat-bog cores. However, we confirm that the stepwise changes apparent in our cumulative cryptotephra curves are not likely to have resulted solely from site-derived biases. Some other process is at play, suggesting the suitability of a regime shift model.

Although wider environmental factors such as frozen lake surfaces or snow drifts, which are known to affect tephra deposition (Bergman et al., 2004; Boygle, 1999), may have been more influential during cold periods of the

late Pleistocene, cryptotephra deposits are routinely identified at high-latitudes affected by these conditions today (e.g., Davies et al., 2021; Monteath et al., 2017). Therefore, it is unlikely that these environmental processes can explain the absence/reduction of cryptotephra deposits across all the different study sites during this period.

A final possible factor is that primary cryptotephra isochrons may be obscured by detrital glass derived from loess deposits in the Great Plains region. This process was noted in Irwin Smith Bog by Jensen et al. (2021) and also affected Long Bog from this study. If the rate of aeolian activity changed during the past, this could bias our records by causing an apparent increase or decrease in the number of observable cryptotephra deposits. However, radiocarbon-dated loess deposits in the Great Plains region suggest that aeolian activity was suppressed between 14,500–10,000 cal yr BP (Mason et al., 2008)—the opposite of what we observe in our records with cryptotephra frequency increasing from ca. 9,000 cal yr BP when detrital glass inputs might be expected to be higher. However, a subtle increase in detrital glass is observed at Long Bog after around 9,000 cal yr BP (Figure S1 in Supporting Information S1) consistent with loess deposition dating by Mason et al. (2008).

4.4. Hypothesis 4: The Increase in the Frequency of Cryptotephra Deposits Was Caused by Changes in Atmospheric Circulation

The increase in the frequency of cryptotephra deposits after ca. 9,000 cal yr BP may be explained by a shift in atmospheric circulations patterns toward a state that favored tephra transport to northeastern North America. Other paleo studies support this supposition and the uptick in cryptotephra deposition starts shortly after several regional proxy records indicate an environmental shift linked with atmospheric circulation and precipitation changes (e.g., Dean et al., 2002; Williams et al., 2010). The relatively short lag between this shift (ca. 8,200 cal yr BP) and the first Mid Holocene deposition of cryptotephra in northeastern North America (ca. 7,860 cal yr BP) is likely to be caused by natural intervals between explosive eruptions.

Evidence for regional atmospheric changes and shifts in aridity ca. 8,200 cal yr BP are expressed in lake-sediment geochemistry (Dean et al., 2002; Nelson & Hu, 2008) and regional pollen, isotopic, aeolian, and paleohydrological records (Finkenbinder et al., 2016, Figure 4; Shuman et al., 2002; Williams et al., 2010). The rapid collapse of the Laurentide Ice Sheet has been suggested as a driver for some of these changes in atmospheric circulation patterns and airflow strength (Bartlein et al., 2014; Shuman et al., 2002), and was advocated by Pyne-O'Donnell et al. (2012) to explain the sudden appearance of Mid Holocene cryptotephra deposits in Nordan's Pond Bog, Newfoundland. Although already greatly reduced in size by the Early Holocene, the topography of the ice sheet continued to impact atmospheric circulation patterns in the North American North Atlantic region until ~8,500 cal yr BP (e.g., Bartlein et al., 2014; Gregoire et al., 2018). Modeling studies, loess deposits, and dated sand spits from paleo lakes at the margins of the former Laurentide Ice Sheet provide evidence for anticyclonic winds over the ice sheet that may have restricted tephra delivery to northeastern North America by promoting regionally dominant easterlies (Bromwich et al., 2004; Pausata et al., 2011; Schaetzl et al., 2016, 2018). These winds, however, are suggested to have been restricted to a narrow belt (~150 km) around the ice sheet margin at near surface levels (Arbogast et al., 2015) and may not have affected more southerly study sites from our data set. However, Dean et al. (2002) and Kirby et al. (2002) both suggest the position of the winter-polar front lay further south during the Early Holocene, facilitating intrusions of Arctic air masses into northeastern North America, pushing the jet stream south and potentially blocking tephra from the North Pacific region from reaching our study sites. For similar reasons, disruption of tephra delivery may have occurred 'upstream' of our study region at the western margins of the Laurentide Ice Sheet, impeding ash plumes extending from Alaska or Kamchatka (Lora et al., 2016). This would explain the absence of tephra from Alaska or Kamchatka sources at this time but allow for the deposition of late Pleistocene tephra associated with Glacier Peak and Mt. St. Helens (Pyne-O'Donnell et al., 2016), both sourced from more southerly locations in the Cascades Range.

Based on the available data and supporting literature discussed above, our findings and analysis support the hypothesis that the observed increase in the frequency of cryptotephra deposits reflects changes in atmospheric circulation. The most likely driver for this change is the final collapse of Laurentide Ice Sheet around 8,000 cal yr BP (e.g., Ullman et al., 2016).

4.5. The Value of Tephrostratigraphic Frameworks Beyond Chronology

The apparent link between the frequency of tephra deposition in northeastern North America and regional climate suggests distal cryptotephra frameworks can provide new data for comparison with paleosimulations of

atmospheric circulation. For example, our results provide evidence that the ice sheet influenced areas further south than (some) models and proxy data suggest (e.g., Arbogast et al., 2015). Although it is difficult to test our hypotheses further with the current data, our results generate interesting scientific questions regarding cryosphere/atmosphere interactions that can be addressed by future studies and new generations of Earth System models. In itself, this demonstrates the value of interrogating patterns in tephrostratigraphic frameworks and considering environmental and depositional information preserved by tephra (Dugmore et al., 2020). We also note that our study includes findings from cryptotephra investigations that were previously considered unsuccessful because of an apparent absence of primary airfall tephra deposits (e.g., Appleman Lake, Silver Lake and Long Bog). These records become key sources of information when considered as part of a wider pattern and reiterate the importance of reporting ‘failed’ results. Information regarding the absence of tephra not only helps to reveal temporal patterns but provides data points in constraining isopach maps and subsequent eruption volume estimates (Cashman & Rust, 2020; Davies et al., 2010).

5. Conclusions

We present five new ultra-distal cryptotephra records from northeastern North America and combine our findings with a review of the existing regional tephrostratigraphy. Our records include further occurrences of well characterized and widespread cryptotephra deposits in northeastern North America (Mt. St. Helens We, Jala pumice, WRAe, Ruppert tephra, Mt. St. Helens Yn and Mazama Ash). Breakpoint analysis of our combined database shows an increase in the frequency of cryptotephra deposits shortly before the Early to Mid Holocene transition, ca. 8,200 cal yr BP. The available evidence suggests this increase is unlikely to have been caused by enhanced volcanic activity, study site availability, or taphonomic bias. Instead, it is best explained by a reorganization in atmospheric circulation associated with the final retreat of the Laurentide Ice Sheet. Exploring the subtleties in these records could provide new data for comparison with paleosimulations of atmospheric circulation. This novel study of long-term ultra-distal tephra deposition highlights the value using tephrostratigraphic frameworks to raise and address scientific questions beyond traditional correlative and dating studies.

Data Availability Statement

All new data used generated by this study is available in Supplementary Data. Example OxCal code is provided in Supplementary Text. R code is available in Supplementary Data.

References

- Arbogast, A. F., Luehmann, M. D., Miller, B. A., Wernette, P. A., Adams, K. M., Waha, J. D., et al. (2015). Late-Pleistocene paleowinds and aeolian sand mobilization in north-central Lower Michigan. *Aeolian Research*, 16, 109–116. <https://doi.org/10.1016/j.aeolia.2014.08.006>
- Bartlein, P. J., Hostetler, S. W., & Alder, J. R. (2014). Paleoclimate. In G. Ohring (Ed.), *Climate change in North America. Regional climate studies*. Springer. https://doi.org/10.1007/978-3-319-03768-4_1
- Bergman, J., Wastegård, S., Hammarlund, D., Wohlfarth, B., & Roberts, S. J. (2004). Holocene tephra horizons at Klocka bog, west-central Sweden: Aspects of reproducibility in subarctic peat deposits. *Journal of Quaternary Science*, 19(3), 241–249. <https://doi.org/10.1002/jqs.833>
- Blockley, S. P., Pyne-O'Donnell, S. D., Lowe, J. J., Matthews, I. P., Stone, A., Pollard, A. M., et al. (2005). A new and less destructive laboratory procedure for the physical separation of distal glass tephra shards from sediments. *Quaternary Science Reviews*, 24(16–17), 1952–1960. <https://doi.org/10.1016/j.quascirev.2004.12.008>
- Blundell, A., Hughes, P. D., & Chambers, F. M. (2018). An 8000-year multi-proxy peat-based palaeoclimate record from Newfoundland: Evidence of coherent changes in bog surface wetness and ocean circulation. *The Holocene*, 28(5), 791–805. <https://doi.org/10.1177/0959683617744261>
- Boyle, J. (1999). Variability of tephra in lake and catchment sediments, Svinavatn, Iceland. *Global and Planetary Change*, 21(1–3), 129–149. [https://doi.org/10.1016/S0921-8181\(99\)00011-9](https://doi.org/10.1016/S0921-8181(99)00011-9)
- Braitseva, O. A., Melekestsev, I. V., Ponomareva, V. V., & Sulerzhitsky, L. D. (1995). Ages of calderas, large explosive craters and active volcanoes in the Kuril-Kamchatka region, Russia. *Bulletin of Volcanology*, 57(6), 383–402. <https://doi.org/10.1007/BF00300984>
- Bromwich, D. H., Toracinta, E. R., Wei, H., Ogleby, R. J., Fastook, J. L., & Hughes, T. J. (2004). Polar MM5 simulations of the winter climate of the Laurentide ice sheet at the LGM. *Journal of Climate*, 17(17), 3415–3433. [https://doi.org/10.1175/1520-0442\(2004\)017<3415:PMSOTW>2.0.CO;2](https://doi.org/10.1175/1520-0442(2004)017<3415:PMSOTW>2.0.CO;2)
- Bronk Ramsey, C. (2009a). OxCal radiocarbon calibration: 2024 release (version 4.4). [Software] <https://c14.arch.ox.ac.uk/oxcal.html>
- Bronk Ramsey, C. B. (2009b). Bayesian analysis of radiocarbon dates. *Radiocarbon*, 51(1), 337–360. <https://doi.org/10.1017/S0038222000033865>
- Brown, S. K., Crosswell, H. S., Sparks, R. S. J., Cottrell, E., Deligne, N. I., Guerrero, N. O., et al. (2014). Characterisation of the quaternary eruption record: Analysis of the large magnitude explosive volcanic eruptions (LaMEVE) database. *Journal of Applied Volcanology*, 3, 1–22. <https://doi.org/10.1186/2191-5040-3-5>
- Buckland, H. M., Cashman, K. V., Engwell, S. L., & Rust, A. C. (2020). Sources of uncertainty in the Mazama isopachs and the implications for interpreting distal tephra deposits from large magnitude eruptions. *Bulletin of Volcanology*, 82(3), 1–17. <https://doi.org/10.1007/s00445-020-1362-1>

Acknowledgments

We thank Chris Hayward and Mike Hall at the Tephrochronology Analytical Unit, University of Edinburgh, for their help and advice with microprobe analysis and stub preparation. Field work and analytical investigations were supported by grants from the Royal Geographical Society (Geographical Club Award), the Explorers Club (The Exploration Fund Grant), and the Geologists Association (New Research Workers award) awarded to Alistair Monteath. EPMA at the University of Alberta was supported by a Natural Sciences and Engineering Research Council of Canada Discovery Grant awarded to Britta Jensen (Grant RGPIN-2018-04926). Data from Petite Bog is an output from a Natural Environment Research Council (NERC) grant: PRECIP project (Grant NE/G019851/1, NE/G02006X/1; NE/G020272/1; NE/G019673/1). Dan Charman, Tim Daley and Will Blake were key PRECIP project members. Charlotte Clarke helped with fieldwork in Newfoundland. Shaun Woudstra assisted with the laboratory preparation of samples. Sandra Nogué, Pete Langdon, and Gill Plunkett kindly commented on a previous draft of this manuscript. Material from Appleman Lake and Silver Lake was provided by the Continental Scientific Drilling Facility, University of Minnesota Twin Cities.

- Bursik, M., Sieh, K., & Meltzner, A. (2014). Deposits of the most recent eruption in the southern Mono craters, California: Description, interpretation and implications for regional marker tephra. *Journal of Volcanology and Geothermal Research*, 275, 114–131. <https://doi.org/10.1016/j.jvolgeores.2014.02.015>
- Cashman, K. V., & Rust, A. C. (2020). Far-travelled ash in past and future eruptions: Combining tephrochronology with volcanic studies. *Journal of Quaternary Science*, 35(1–2), 11–22. <https://doi.org/10.1002/jqs.3159>
- Charman, D. J., Amesbury, M. J., Hinchliffe, W., Hughes, P. D., Mallon, G., Blake, W. H., et al. (2015). Drivers of Holocene peatland carbon accumulation across a climate gradient in north-eastern North America. *Quaternary Science Reviews*, 121, 110–119. <https://doi.org/10.1016/j.quascirev.2015.05.012>
- Coulter, S. E., Pilcher, J. R., Plunkett, G., Baillie, M., Hall, V. A., Steffensen, J. P., et al. (2012). Holocene tephra highlight complexity of volcanic signals in Greenland ice cores. *Journal of Geophysical Research*, 117(D21). <https://doi.org/10.1029/2012JD017698>
- Crowther, H. S., Arora, B., Brown, S. K., Cottrell, E., Deligne, N. I., Guerrero, N. O., et al. (2012). Global database on large magnitude explosive volcanic eruptions (LaMEVE). *Journal of Applied Volcanology*, 1, 1–13. <https://doi.org/10.1186/2191-5040-1-4>
- Dalton, A. S., Margold, M., Stokes, C. R., Tarasov, L., Dyke, A. S., Adams, R. S., et al. (2020). An updated radiocarbon-based ice margin chronology for the last deglaciation of the North American Ice Sheet Complex. *Quaternary Science Reviews*, 234, 106223. <https://doi.org/10.1016/j.quascirev.2020.106223>
- Davies, L. J., Jensen, B. J., Froese, D. G., & Wallace, K. L. (2016). Late Pleistocene and Holocene tephrostratigraphy of interior Alaska and Yukon: Key beds and chronologies over the past 30,000 years. *Quaternary Science Reviews*, 146, 28–53. <https://doi.org/10.1016/j.quascirev.2016.05.026>
- Davies, L. J., Jensen, B. J., & Kaufman, D. S. (2021). Late Holocene cryptotephra from Cascade Lake, Alaska: Supporting data for a 21,000-year multi-chronometer Bayesian age model. *Geochronology Discussions*, 2021, 1–35. <https://doi.org/10.5194/gchron-4-121-2022>
- Davies, S. M., Hoek, W. Z., Bohncke, S. J., Lowe, J. J., Pyne-O'Donnell, S. P., & Turney, C. S. (2005). Detection of Lateglacial distal tephra layers in The Netherlands. *Boreas*, 34(2), 123–135. <https://doi.org/10.1111/j.1502-3885.2005.tb01010.x>
- Davies, S. M., Larsen, G., Wastegård, S., Turney, C. S., Hall, V. A., Coyle, L., & Thordarson, T. (2010). Widespread dispersal of Icelandic tephra: How does the Eyjafjöll eruption of 2010 compare to past Icelandic events? *Journal of Quaternary Science*, 25(5), 605–611. <https://doi.org/10.1002/jqs.1421>
- Dean, W. E., Forester, R. M., & Bradbury, J. P. (2002). Early Holocene change in atmospheric circulation in the northern Great Plains: An upstream view of the 8.2 ka cold event. *Quaternary Science Reviews*, 21(16–17), 1763–1775. [https://doi.org/10.1016/S0277-3791\(02\)00002-1](https://doi.org/10.1016/S0277-3791(02)00002-1)
- de Fontaine, C. S., Kaufman, D. S., Anderson, R. S., Werner, A., Waythomas, C. F., & Brown, T. A. (2007). Late Quaternary distal tephra-fall deposits in lacustrine sediments, Kenai Peninsula, Alaska. *Quaternary Research*, 68(1), 64–78. <https://doi.org/10.1016/j.yqres.2007.03.006>
- Dugmore, A. (1989). Icelandic volcanic ash in Scotland. *Scottish Geographical Magazine*, 105(3), 168–172. <https://doi.org/10.1080/14702548908554430>
- Dugmore, A. J., Larsen, G. R., & Newton, A. J. (1995). Seven tephra isochrones in Scotland. *The Holocene*, 5(3), 257–266. <https://doi.org/10.1177/095968369500500301>
- Dugmore, A. J., Thompson, P. I., Streeter, R. T., Cutler, N. A., Newton, A. J., & Kirkbride, M. P. (2020). The interpretative value of transformed tephra sequences. *Journal of Quaternary Science*, 35(1–2), 23–38. <https://doi.org/10.1002/jqs.3174>
- Eden, D. N., Froggatt, P. C., & McIntosh, P. D. (1992). The distribution and composition of volcanic glass in late Quaternary loess deposits of southern South Island, New Zealand, and some possible correlations. *New Zealand Journal of Geology and Geophysics*, 35(1), 69–79. <https://doi.org/10.1080/00288306.1992.9514501>
- Finkenbinder, M. S., Abbott, M. B., & Steinman, B. A. (2016). Holocene climate change in Newfoundland reconstructed using oxygen isotope analysis of lake sediment cores. *Global and Planetary Change*, 143, 251–261. <https://doi.org/10.1016/j.gloplacha.2016.06.014>
- Fontijn, K., Lachowycz, S. M., Rawson, H., Pyle, D. M., Mather, T. A., Naranjo, J. A., & Moreno-Roa, H. (2014). Late Quaternary tephrostratigraphy of southern Chile and Argentina. *Quaternary Science Reviews*, 89, 70–84. <https://doi.org/10.1016/j.quascirev.2014.02.007>
- Gill, J. L., Williams, J. W., Jackson, S. T., Donnelly, J. P., & Schellinger, G. C. (2012). Climatic and megaherbivory controls on late-glacial vegetation dynamics: A new, high-resolution, multi-proxy record from Silver Lake, Ohio. *Quaternary Science Reviews*, 34, 66–80. <https://doi.org/10.1016/j.quascirev.2011.12.008>
- Gill, J. L., Williams, J. W., Jackson, S. T., Lininger, K. B., & Robinson, G. S. (2009). Pleistocene megafaunal collapse, novel plant communities, and enhanced fire regimes in North America. *Science*, 326(5956), 1100–1103. <https://doi.org/10.1126/science.1179504>
- Global volcanism Program. (2018). Smithsonian Institution. Retrieved from <https://volcano.si.edu/> 15 March 2019.
- Gregoire, L. J., Ivanovic, R. F., Maycock, A. C., Valdes, P. J., & Stevenson, S. (2018). Holocene lowering of the Laurentide ice sheet affects North Atlantic gyre circulation and climate. *Climate Dynamics*, 51(9), 3797–3813. <https://doi.org/10.1007/s00382-018-4111-9>
- Hayward, C. (2012). High spatial resolution electron probe microanalysis of tephra and melt inclusions without beam-induced chemical modification. *The Holocene*, 22(1), 119–125. <https://doi.org/10.1177/0959683611409777>
- Hildreth, W. (2007). *Quaternary magmatism in the Cascades — geologic perspectives* (p. 1744). USGS Professional Paper.
- Jensen, B. J., Pyne-O'Donnell, S., Plunkett, G., Froese, D. G., Hughes, P. D., Sigl, M., et al. (2014). Transatlantic distribution of the Alaskan White River Ash. *Geology*, 42(10), 875–878. <https://doi.org/10.1130/G35945.1>
- Jensen, B. J. L., Davies, L. D., Nolan, C., Pyne-O'Donnell, S., Monteath, A. J., Ponomareva, V., et al. (2021). A latest Pleistocene and Holocene composite tephrostratigraphic framework for north-eastern North America. *Quaternary Science Reviews*, 272, 107242. <https://doi.org/10.1016/j.quascirev.2021.107242>
- Jones, G., Davies, S. M., Staff, R. A., Loader, N. J., Davies, S. J., & Walker, M. J. (2020). Traces of volcanic ash from the Mediterranean, Iceland and North America in a Holocene record from south Wales, UK. *Journal of Quaternary Science*, 35(1–2), 163–174. <https://doi.org/10.1002/jqs.3141>
- Jull, M., & McKenzie, D. (1996). The effect of deglaciation on mantle melting beneath Iceland. *Journal of Geophysical Research*, 101(B10), 21815–21828. <https://doi.org/10.1029/96JB01308>
- Kinder, M., Wulf, S., Appelt, O., Hardiman, M., Zarczyński, M., & Tylmann, W. (2020). Late-Holocene ultra-distal cryptotephra discoveries in varved sediments of Lake Żabińskie, NE Poland. *Journal of Volcanology and Geothermal Research*, 402, 106988. <https://doi.org/10.1016/j.jvolgeores.2020.106988>
- Kirby, M. E., Mullins, H. T., Patterson, W. P., & Burnett, A. W. (2002). Late glacial–Holocene atmospheric circulation and precipitation in the northeast United States inferred from modern calibrated stable oxygen and carbon isotopes. *GSA Bulletin*, 114(10), 1326–1340. [https://doi.org/10.1130/0016-7606\(2002\)114<1326:LGHACA>2.0.CO;2](https://doi.org/10.1130/0016-7606(2002)114<1326:LGHACA>2.0.CO;2)
- Kyle, P. R., Ponomareva, V. V., & Rourke Schlupe, R. (2011). Geochemical characterization of marker tephra layers from major Holocene eruptions, Kamchatka Peninsula, Russia. *International Geology Review*, 53(9), 1059–1097. <https://doi.org/10.1080/00206810903442162>

- Lacasse, C. (2001). Influence of climate variability on the atmospheric transport of Icelandic tephra in the subpolar North Atlantic. *Global and Planetary Change*, 29(1–2), 31–55. [https://doi.org/10.1016/S0921-8181\(01\)00099-6](https://doi.org/10.1016/S0921-8181(01)00099-6)
- Lawson, I. T., Swindles, G. T., Plunkett, G., & Greenberg, D. (2012). The spatial distribution of Holocene cryptotephra in north-west Europe since 7 ka: Implications for understanding ash fall events from Icelandic eruptions. *Quaternary Science Reviews*, 41, 57–66. <https://doi.org/10.1016/j.quascirev.2012.02.018>
- Lora, J. M., Mitchell, J. L., & Tripathi, A. E. (2016). Abrupt reorganization of North Pacific and western North American climate during the last deglaciation. *Geophysical Research Letters*, 43(22), 11–796. <https://doi.org/10.1002/2016GL071244>
- Lowe, D. J. (2011). Tephrochronology and its application: A review. *Quaternary Geochronology*, 6(2), 107–153. <https://doi.org/10.1016/j.quageo.2010.08.003>
- Lowe, D. J., & Hunt, J. B. (2001). A summary of terminology used in tephra-related studies. *Les Dossiers de l'Archéologie*, 1, 17–22. <https://hdl.handle.net/10289/3526>
- Lowe, D. J., Pearce, N. J., Jorgensen, M. A., Kuehn, S. C., Tryon, C. A., & Hayward, C. L. (2017). Correlating tephra and cryptotephra using glass compositional analyses and numerical and statistical methods: Review and evaluation. *Quaternary Science Reviews*, 175, 1–44. <https://doi.org/10.1016/j.quascirev.2017.08.003>
- Lowe, D. J., Shane, P. A., Alloway, B. V., & Newnham, R. M. (2008). Fingerprints and age models for widespread New Zealand tephra marker beds erupted since 30,000 years ago: A framework for NZ-INTIMATE. *Quaternary Science Reviews*, 27(1–2), 95–126. <https://doi.org/10.1016/j.quascirev.2007.01.013>
- Mackay, H., Hughes, P. D. M., Jensen, B. J. L., Langdon, P. G., Pyne-O'Donnell, S., Plunkett, G., et al. (2016). The foundations of a late Holocene tephrostratigraphic framework for eastern North America. *Quaternary Science Reviews*, 132, 101–113. <https://doi.org/10.1016/j.quascirev.2015.11.011>
- Mackay, H., Plunkett, G., Jensen, B., Aubry, T., Corona, C., Kim, W., et al. (2022). The 853 CE Mount Churchill eruption: Examining the potential climatic and societal impacts and the timing of the medieval climate anomaly in the North Atlantic region. *Climate of the Past*, 18(6), 1475–1508. <https://doi.org/10.5194/cp-18-1475-2022>
- Mason, J. A., Miao, X., Hanson, P. R., Johnson, W. C., Jacobs, P. M., & Goble, R. J. (2008). Loess record of the Pleistocene–Holocene transition on the northern and central Great Plains, USA. *Quaternary Science Reviews*, 27(17–18), 1772–1783. <https://doi.org/10.1016/j.quascirev.2008.07.004>
- Miller, T. P., & Smith, R. L. (1987). Late Quaternary caldera-forming eruptions in the eastern Aleutian arc, Alaska. *Geology*, 15(5), 434–438. [https://doi.org/10.1130/0091-7613\(1987\)15<434:LQCEIT>2.0.CO;2](https://doi.org/10.1130/0091-7613(1987)15<434:LQCEIT>2.0.CO;2)
- Monteath, A. J., Bolton, M., Harvey, J., Seidenkrantz, M. S., Pearce, C., & Jensen, B. (2023). Ultra-distal tephra deposits and Bayesian modelling constrain a variable marine radiocarbon offset in Placentia Bay, Newfoundland. *Geochronology*, 5(1), 229–240. <https://doi.org/10.5194/gchron-5-229-2023>
- Monteath, A. J., Hughes, P. D. M., & Wastegård, S. (2019). Evidence for distal transport of reworked Andean tephra: Extending the cryptotephra framework from the Austral volcanic zone. *Quaternary Geochronology*, 51, 64–71. <https://doi.org/10.1016/j.quageo.2019.01.003>
- Monteath, A. J., Teuten, A. E., Hughes, P. D. M., & Wastegård, S. (2019). The effects of the peat acid digestion protocol on geochemically and morphologically diverse tephra deposits. *Journal of Quaternary Science*, 34(4–5), 269–274. <https://doi.org/10.1002/jqs.3104>
- Monteath, A. J., van Hardenbroek, M., Davies, L. J., Froese, D. G., Langdon, P. G., Xu, X., & Edwards, M. E. (2017). Chronology and glass chemistry of tephra and cryptotephra horizons from lake sediments in northern Alaska, USA. *Quaternary Research*, 88(2), 169–178. <https://doi.org/10.1017/qua.2017.38>
- Muggeo, V. M. (2020). Selecting number of breakpoints in segmented regression: Implementation in the R package segmented. *Technical report*.
- Muggeo, V. M. R. (2003). Estimating regression models with unknown break-points. *Statistics in Medicine*, 22(19), 3055–3071. <https://doi.org/10.1002/sim.1545>
- Muggeo, V. M. R. (2008). Segmented: An R package to fit regression models with broken-line relationships. *R News*, 8(1), 20–25.
- Mullineaux, D. R. (1996). Pre-1980 tephra-fall deposits erupted from Mount St. Helens. *U. S. Geological Survey Professional Paper*, 1563. <https://doi.org/10.3133/pp1563>
- Narcisi, B., Petit, J. R., Delmonte, B., Basile-Doelsch, I., & Maggi, V. (2005). Characteristics and sources of tephra layers in the EPICA-Dome C ice record (east Antarctica): Implications for past atmospheric circulation and ice core stratigraphic correlations. *Earth and Planetary Science Letters*, 239(3–4), 253–265. <https://doi.org/10.1016/j.epsl.2005.09.005>
- Narcisi, B., Petit, J. R., Delmonte, B., Scarchilli, C., & Stenni, B. (2012). A 16,000-yr tephra framework for the Antarctic ice sheet: A contribution from the new Talos Dome core. *Quaternary Science Reviews*, 49, 52–63. <https://doi.org/10.1016/j.quascirev.2012.06.011>
- Nelson, D. M., & Hu, F. S. (2008). Patterns and drivers of Holocene vegetational change near the prairie–forest ecotone in Minnesota: Revisiting McAndrews' transect. *New Phytologist*, 179(2), 449–459. <https://doi.org/10.1111/j.1469-8137.2008.02482.x>
- Newhall, C. G., & Self, S. (1982). The volcanic explosivity index (VEI) an estimate of explosive magnitude for historical volcanism. *Journal of Geophysical Research*, 87(C2), 1231–1238. <https://doi.org/10.1029/JC087iC02p01231>
- Pausata, F. S., Li, C., Wettstein, J., Kageyama, M., & Nisancioglu, K. H. (2011). The key role of topography in altering North Atlantic atmospheric circulation during the last glacial period. Past climate variability: Model analysis and proxy intercomparison. *Climate of the Past*, 7(4), 1089–1101. <https://doi.org/10.5194/cp-7-1089-2011>
- Pearce, N. J., Westgate, J. A., Preece, S. J., Eastwood, W. J., & Perkins, W. T. (2004). Identification of Aniakchak (Alaska) tephra in Greenland ice core challenges the 1645 BC date for Minoan eruption of Santorini. *Geochemistry, Geophysics, Geosystems*, 5(3). <https://doi.org/10.1029/2003GC000672>
- Persson, C. (1971). Tephrochronological investigation of peat deposits in Scandinavia and on the Faroe Islands. *Geological Survey of Sweden C*, 656. <http://pascal-francis.inist.fr/vibad/index.php?action=getRecordDetail&idt=GEODEBRGM72220430>
- Pilcher, J. R., & Hall, V. A. (1992). Towards a tephrochronology for the Holocene of the north of Ireland. *The Holocene*, 2(3), 255–259. <https://doi.org/10.1177/095968369200200307>
- Pilcher, J. R., Hall, V. A., & McCormac, F. G. (1995). Dates of Holocene Icelandic volcanic eruptions from tephra layers in Irish peats. *The Holocene*, 5(1), 103–110. <https://doi.org/10.1177/095968369500500111>
- Plunkett, G., & Pilcher, J. R. (2018). Defining the potential source region of volcanic ash in northwest Europe during the Mid-to Late Holocene. *Earth-Science Reviews*, 179, 20–37. <https://doi.org/10.1016/j.earscirev.2018.02.006>
- Plunkett, G. M., Pilcher, J. R., McCormac, F. G., & Hall, V. A. (2004). New dates for first millennium BC tephra isochrones in Ireland. *The Holocene*, 14(5), 780–786. <https://doi.org/10.1191/0959683604hl757rr>
- Ponomareva, V., Portnyagin, M., Pendea, I. F., Zelenin, E., Bourgeois, J., Pinegina, T., & Kozhurin, A. (2017). A full Holocene tephrochronology for the Kamchatka Peninsula region: Applications from Kamchatka to North America. *Quaternary Science Reviews*, 168, 101–122. <https://doi.org/10.1016/j.quascirev.2017.04.031>

- Portnyagin, M. V., Ponomareva, V. V., Zelenin, E. A., Bazanova, L. I., Pevzner, M. M., Plechova, A. A., et al. (2020). TephraKam: Geochemical database of glass compositions in tephra and welded tuffs from the Kamchatka volcanic arc (northwestern Pacific). *Earth System Science Data*, 12(1), 469–486. <https://doi.org/10.5194/essd-12-469-2020>
- Praetorius, S., Mix, A., Jensen, B., Froese, D., Milne, G., Wolhowe, M., et al. (2016). Interaction between climate, volcanism, and isostatic rebound in Southeast Alaska during the last deglaciation. *Earth and Planetary Science Letters*, 452, 79–89. <https://doi.org/10.1016/j.epsl.2016.07.033>
- Pyne-O'Donnell, S. D., Cwynar, L. C., Jensen, B. J., Vincent, J. H., Kuehn, S. C., Spear, R., & Froese, D. G. (2016). West Coast volcanic ashes provide a new continental-scale Lateglacial isochron. *Quaternary Science Reviews*, 142, 16–25. <https://doi.org/10.1016/j.quascirev.2016.04.014>
- Pyne-O'Donnell, S. D., & Jensen, B. J. (2020). Glacier peak and mid-Lateglacial Katla cryptotephra in Scotland: Potential new intercontinental and marine-terrestrial correlations. *Journal of Quaternary Science*, 35(1–2), 155–162. <https://doi.org/10.1002/jqs.3171>
- Pyne-O'Donnell, S. D. F. (2011). The taphonomy of Last Glacial–Interglacial Transition (LGIT) distal volcanic ash in small Scottish lakes. *Boreas*, 40(1), 131–145. <https://doi.org/10.1111/j.1502-3885.2010.00154.x>
- Pyne-O'Donnell, S. D. F., Hughes, P. D. M., Froese, D. G., Jensen, B. J. L., Kuehn, S. C., Mallon, G., et al. (2012). High-precision ultra-distal Holocene tephrochronology in North America. *Quaternary Science Reviews*, 52, 6–11. <https://doi.org/10.1016/j.quascirev.2012.07.024>
- Rabett, R. J., Pryor, A. J. E., Simpson, D. J., Farr, L. R., Pyne-O'Donnell, S., Blaauw, M., et al. (2019). A multi-proxy reconstruction of environmental change in the vicinity of the North Bay outlet of pro-glacial Lake Algonquin. *Open Quaternary*, 5, 1–27. <https://doi.org/10.5334/oq.54>
- Reimer, P. J., Austin, W. E., Bard, E., Bayliss, A., Blackwell, P. G., Ramsey, C. B., et al. (2020). The IntCal20 Northern Hemisphere radiocarbon age calibration curve (0–55 cal kBP). *Radiocarbon*, 62(4), 725–757. <https://doi.org/10.1017/RDC.2020.41>
- Saxby, J., Rust, A., Cashman, K., & Beckett, F. (2020). The importance of grain size and shape in controlling the dispersion of the Vedde cryptotephra. *Journal of Quaternary Science*, 35(1–2), 175–185. <https://doi.org/10.1002/jqs.3152>
- Schaetzl, R. J., Krist, F. J., Lewis, C. M., Luehmann, M. D., & Michalek, M. J. (2016). Spits formed in glacial Lake Algonquin indicate strong easterly winds over the Laurentian Great lakes during late Pleistocene. *Journal of Paleolimnology*, 55(1), 49–65. <https://doi.org/10.1007/s10933-015-9862-2>
- Schaetzl, R. J., Larson, P. H., Faulkner, D. J., Running, G. L., Jol, H. M., & Rittenour, T. M. (2018). Eolian sand and loess deposits indicate west-northwest paleowinds during the Late Pleistocene in western Wisconsin, USA. *Quaternary Research*, 89(3), 769–785. <https://doi.org/10.1017/qua.2017.88>
- Shuman, B., Bartlein, P., Logan, N., Newby, P., & Webb, I. I. T. (2002). Parallel climate and vegetation responses to the early Holocene collapse of the Laurentide Ice Sheet. *Quaternary Science Reviews*, 21(16–17), 1793–1805. [https://doi.org/10.1016/S0277-3791\(02\)00025-2](https://doi.org/10.1016/S0277-3791(02)00025-2)
- Sigl, M., Toohey, M., McConnell, J. R., Cole-Dai, J., & Severi, M. (2022). Volcanic stratospheric sulfur injections and aerosol optical depth during the Holocene (past 11,500 years) from a bipolar ice core array. *Earth System Science Data Discussions*, 14(7), 3167–3196. <https://doi.org/10.5194/essd-14-3167-2022>
- Spano, N. G., Lane, C. S., Francis, S. W., & Johnson, T. C. (2017). Discovery of Mount Mazama cryptotephra in Lake superior (North America): Implications and potential applications. *Geology*, 45(12), 1071–1074. <https://doi.org/10.1130/G39394.1>
- Sulpizio, R., Zanchetta, G., Caron, B., Dellino, P., Mele, D., Giaccio, B., et al. (2014). Volcanic ash hazard in the Central Mediterranean assessed from geological data. *Bulletin of Volcanology*, 76(10), 1–8. <https://doi.org/10.1007/s00445-014-0866-y>
- Swindles, G. T., Lawson, I. T., Savov, I. P., Connor, C. B., & Plunkett, G. (2011). A 7000 yr perspective on volcanic ash clouds affecting northern Europe. *Geology*, 39(9), 887–890. <https://doi.org/10.1130/G32146.1>
- Swindles, G. T., Watson, E. J., Savov, I. P., Lawson, I. T., Schmidt, A., Hooper, A., et al. (2018). Climatic control on Icelandic volcanic activity during the mid-Holocene. *Geology*, 46(1), 47–50. <https://doi.org/10.1130/G39633.1>
- Thorarinsson, S. (1981). Tephra studies and tephrochronology: A historical review with special reference to Iceland. In S. Self & R. S. J. Sparks (Eds.), *Tephra studies*. Springer. https://doi.org/10.1007/978-94-009-8537-7_1
- Timms, R. G., Matthews, I. P., Lowe, J. J., Palmer, A. P., Weston, D. J., MacLeod, A., & Blockley, S. P. (2019). Establishing tephrostratigraphic frameworks to aid the study of abrupt climatic and glacial transitions: A case study of the last glacial-interglacial transition in the British isles (c. 16–8 ka BP). *Earth-Science Reviews*, 192, 34–64. <https://doi.org/10.1016/j.earscirev.2019.01.003>
- Turney, C. S. M. (1998). Extraction of rhyolitic component of Vedde microtephra from minerogenic lake sediments. *Journal of Paleolimnology*, 19(2), 199–206. <https://doi.org/10.1023/A:1007926322026>
- Ullman, D. J., Carlson, A. E., Hostetler, S. W., Clark, P. U., Cuzzone, J., Milne, G. A., et al. (2016). Final Laurentide ice-sheet deglaciation and Holocene climate-sea level change. *Quaternary Science Reviews*, 152, 49–59. <https://doi.org/10.1016/j.quascirev.2016.09.014>
- Walker, M., Head, M. J., Lowe, J., Berkelhammer, M., Björck, S., Cheng, H., et al. (2019). Subdividing the Holocene series/Epoch: Formalization of stages/ages and subseries/subepochs, and designation of GSSPs and auxiliary stratotypes. *Journal of Quaternary Science*, 34(3), 173–186. <https://doi.org/10.1002/jqs.3097>
- Watson, E. J., Kolaczek, P., Słowiński, M., Swindles, G. T., Marcisz, K., Gałka, M., & Lamentowicz, M. (2017). First discovery of Holocene Alaskan and Icelandic tephra in Polish peatlands. *Journal of Quaternary Science*, 32(4), 457–462. <https://doi.org/10.1002/jqs.2945>
- Watson, E. J., Swindles, G. T., Lawson, I. T., & Savov, I. P. (2016). Do peatlands or lakes provide the most comprehensive distal tephra records? *Quaternary Science Reviews*, 139, 110–128. <https://doi.org/10.1016/j.quascirev.2016.03.011>
- Watson, E. J., Swindles, G. T., Lawson, I. T., Savov, I. P., & Wastegård, S. (2017). The presence of Holocene cryptotephra in Wales and southern England. *Journal of Quaternary Science*, 32(4), 493–500. <https://doi.org/10.1002/jqs.2942>
- Watson, E. J., Swindles, G. T., Savov, I. P., Lawson, I. T., Connor, C. B., & Wilson, J. A. (2017). Estimating the frequency of volcanic ash clouds over northern Europe. *Earth and Planetary Science Letters*, 460, 41–49. <https://doi.org/10.1016/j.epsl.2016.11.054>
- Watt, S. F., Pyle, D. M., & Mather, T. A. (2013). The volcanic response to deglaciation: Evidence from glaciated arcs and a reassessment of global eruption records. *Earth-Science Reviews*, 122, 77–102. <https://doi.org/10.1016/j.earscirev.2013.03.007>
- Williams, J. W., Shuman, B., Bartlein, P. J., Diffenbaugh, N. S., & Webb, T. (2010). Rapid, time-transgressive, and variable responses to early Holocene midcontinental drying in North America. *Geology*, 38(2), 135–138. <https://doi.org/10.1130/G30413.1>
- Zdanowicz, C. M., Zielinski, G. A., & Germani, M. S. (1999). Mount Mazama eruption: Calendrical age verified and atmospheric impact assessed. *Geology*, 27(7), 621–624. [https://doi.org/10.1130/0091-7613\(1999\)027<0621:MMECAV>2.3.CO;2](https://doi.org/10.1130/0091-7613(1999)027<0621:MMECAV>2.3.CO;2)
- Zielinski, G. A., Mayewski, P. A., Meeker, L. D., Grönvold, K., Germani, M. S., Whitlow, S., et al. (1997). Volcanic aerosol records and tephrochronology of the Summit, Greenland, ice cores. *Journal of Geophysical Research*, 102(C12), 26625–26640. <https://doi.org/10.1029/96JC03547>
- Zielinski, G. A., Mayewski, P. A., Meeker, L. D., Whitlow, S., & Twickler, M. S. (1996). A 110,000-yr record of explosive volcanism from the GISP2 (Greenland) ice core. *Quaternary Research*, 45(2), 109–118. <https://doi.org/10.1006/qres.1996.0013>

References From the Supporting Information

- Bacon, C. R., & Lanphere, M. A. (2006). Eruptive history and geochronology of Mount Mazama and the crater lake region, Oregon. *Geological Society of America Bulletin*, 118(11–12), 1331–1359. <https://doi.org/10.1130/B25906.1>
- Bourne, A. J., Abbott, P. M., Albert, P. G., Cook, E., Pearce, N. J. G., Ponomareva, V., et al. (2016). Underestimated risks of recurrent long-range ash dispersal from northern Pacific Arc volcanoes. *Scientific Reports*, 6(1), 29837. <https://doi.org/10.1038/srep29837>
- Bronk Ramsey, C. B. (2008). Deposition models for chronological records. *Quaternary Science Reviews*, 27(1–2), 42–60. <https://doi.org/10.1016/j.quascirev.2007.01.019>
- Bronk Ramsey, C. B. (2009b). Dealing with outliers and offsets in radiocarbon dating. *Radiocarbon*, 51(3), 1023–1045. <https://doi.org/10.1017/S0033822200034093>
- Bronk Ramsey, C. B., & Lee, S. (2013). Recent and planned developments of the program OxCal. *Radiocarbon*, 55(2), 720–730. <https://doi.org/10.1017/S0033822200057878>
- Chagué-Goff, C., & Fyfe, W. S. (1996). Geochemical and petrographical characteristics of a domed bog, Nova Scotia: A modern analogue for temperate coal deposits. *Organic Geochemistry*, 24(2), 141–158. [https://doi.org/10.1016/0146-6380\(96\)00014-9](https://doi.org/10.1016/0146-6380(96)00014-9)
- Daley, T. J., Street-Perrott, F. A., Loader, N. J., Barber, K. E., Hughes, P. D., Fisher, E. H., & Marshall, J. D. (2009). Terrestrial climate signal of the “8200 yr BP cold event” in the Labrador Sea region. *Geology*, 37(9), 831–834. <https://doi.org/10.1130/G30043A.1>
- Davies, L. J. (2018). *The development of a Holocene cryptotephra framework in northwestern North America*. University of Alberta. Unpublished PhD. <https://doi.org/10.7939/R3HX1660C>
- Egan, J., Staff, R., & Blackford, J. (2015). A high-precision age estimate of the Holocene Plinian eruption of Mount Mazama, Oregon, USA. *The Holocene*, 25(7), 1054–1067. <https://doi.org/10.1177/0959683615576230>
- Foo, Z. H., Jensen, B. J., & Bolton, M. S. (2020). Glass geochemical compositions from widespread tephra erupted over the last 200 years from Mount St. Helens. *Journal of Quaternary Science*, 35(1–2), 102–113. <https://doi.org/10.1002/jqs.3166>
- Hall, M., & Hayward, C. (2014). Preparation of micro-and crypto-tephras for quantitative microbeam analysis. *Geological Society, London, Special Publications*, 398(1), 21–28. <https://doi.org/10.1144/SP398.5>
- Hughes, P. D., Blundell, A., Charman, D. J., Bartlett, S., Daniell, J. R., Wojatschke, A., & Chambers, F. M. (2006). An 8500 cal. Year multi-proxy climate record from a bog in eastern Newfoundland: Contributions of meltwater discharge and solar forcing. *Quaternary Science Reviews*, 25(11–12), 1208–1227. <https://doi.org/10.1016/j.quascirev.2005.11.001>
- Jensen, B. J., Froese, D. G., Preece, S. J., Westgate, J. A., & Stachel, T. (2008). An extensive middle to late Pleistocene tephrochronologic record from east-central Alaska. *Quaternary Science Reviews*, 27(3–4), 411–427. <https://doi.org/10.1016/j.quascirev.2007.10.010>
- Jensen, B. J., Beaudoin, A. B., Clynne, M. A., Harvey, J., & Vallance, J. W. (2019). A re-examination of the three most prominent Holocene tephra deposits in western Canada: Bridge River, Mount St. Helens Yn and Mazama. *Quaternary International*, 500, 83–95. <https://doi.org/10.1016/j.quaint.2019.03.017>
- Kuehn, S. C., Froese, D. G., & Shane, P. A. (2011). The INTAV intercomparison of electron-beam microanalysis of glass by tephrochronology laboratories: Results and recommendations. *Quaternary International*, 246(1–2), 19–47. <https://doi.org/10.1016/j.quaint.2011.08.022>
- Lerbekmo, J. F. (2008). The White River Ash: Largest Holocene Plinian tephra. *Canadian Journal of Earth Sciences*, 45(6), 693–700. <https://doi.org/10.1139/E08-023>
- Preece, S. J., McGimsey, R. G., Westgate, J. A., Pearce, N. J. G., Hart, W. K., & Perkins, W. T. (2014). Chemical complexity and source of the White River Ash, Alaska and Yukon. *Geosphere*, 10(5), 1020–1042. <https://doi.org/10.1130/GES00953.1>
- Roland, T. P., Mackay, H., & Hughes, P. D. M. (2015). Tephra analysis in ombrotrophic peatlands: A geochemical comparison of acid digestion and density separation techniques. *Journal of Quaternary Science*, 30(1), 3–8. <https://doi.org/10.1002/jqs.2754>
- Sieron, K., & Siebe, C. (2008). Revised stratigraphy and eruption rates of Ceboruco stratovolcano and surrounding monogenetic vents (Nayarit, Mexico) from historical documents and new radiocarbon dates. *Journal of Volcanology and Geothermal Research*, 176(2), 241–264. <https://doi.org/10.1016/j.jvolgeores.2008.04.006>
- Toohy, M., & Sigl, M. (2017). Volcanic stratospheric sulfur injections and aerosol optical depth from 500 BCE to 1900 CE. *Earth System Science Data*, 9(2), 809–831. <https://doi.org/10.5194/essd-9-809-2017>
- Watson, E. J., Kołaczek, P., Słowiński, M., Swindles, G. T., Marcisz, K., Galka, M., & Lamentowicz, M. (2017). First discovery of Holocene Alaskan and Icelandic tephra in polish peatlands. *Journal of Quaternary Science*, 32(4), 457–462. <https://doi.org/10.1002/jqs.2945>
- Westgate, J. A., & Gorton, M. P. (1981). Correlation techniques in tephra studies. In S. Self & R. S. J. Sparks (Eds.), *Tephra studies. NATO advanced study institutes series* (Vol. 75, pp. 73–94). Springer. https://doi.org/10.1007/978-94-009-8537-7_5
- Yamaguchi, D. K. (1983). New tree-ring dates for recent eruptions of Mount St. Helens. *Quaternary Research*, 20(2), 554–557. [https://doi.org/10.1016/0033-5894\(83\)90080-7](https://doi.org/10.1016/0033-5894(83)90080-7)
- Yamaguchi, D. K. (1985). Tree-ring evidence for a two-year interval between recent prehistoric explosive eruptions of Mount St. Helens. *Geology*, 13(8), 554–557. [https://doi.org/10.1130/0091-7613\(1985\)13<554:TEFATI>2.0.CO;2](https://doi.org/10.1130/0091-7613(1985)13<554:TEFATI>2.0.CO;2)